Submonthly Variability of Convection and Circulation over and around the Tibetan Plateau during the Boreal Summer

Hatsuki FUJINAMI

Core Research for Evolutional Science and Technology, Japan Science and Technology Agency, Kawaguchi, Japan

and

Tetsuzo YASUNARI

Hydrospheric Atmospheric Research Center, Nagoya University, Nagoya, Japan

(Manuscript received 29 September 2003, in final form 31 August 2004)

Abstract

Convective variability at submonthly timescales (7–20 days) over the Tibetan Plateau and the associated large-scale atmospheric circulation and convection were examined over regions affected by the Asian Monsoon. The mature phase of the Asian summer monsoon (July–August) was analyzed for those years (1986, 93, 98) in which convective variability on timescales of 14 days was notable over the Tibetan Plateau.

Composite analyses of OLR, based on the filtered Tbb time series over the southern Tibetan Plateau, show that significant convective signals rotate clockwise around 28°N, 90°E, affecting the Tibetan Plateau, Indochina, the Bay of Bengal, and India. Significant signals also appear around the Philippines and the South China Sea. A well-developed wave train extending from North Africa to far-east Asia along the Asian subtropical jet is associated with convective fluctuations over the plateau. The waves are quasi-stationary and have a Rossby wave-like downward wave train with wavenumber 7.

The waves control convective fluctuations over the plateau. During the transition to active (inactive) convection, an upper-level trough (ridge) develops west of the plateau. Simultaneously, cyclonic anomalies strengthen over India between the lower and middle troposphere. The development of the two troughs induces a southerly flow of moist air toward the plateau. Moistening of the lower atmosphere creates favorable conditions for subsequent active moist convection.

Possible processes for forming the wave train over the subtropical jet and a link for convective signals between midlatitudes and the Asian monsoon are discussed.

1. Introduction

Intraseasonal oscillations (ISOs) of convective activity and the associated atmospheric circulations are prominent phenomena associated with the Asian summer monsoon. Many studies have investigated 30–60-day oscillations, the so-called Madden-Julian Oscillation (MJO) (Madden and Julian 1972), and the relationships between the MJO and the active/break periods of the Asian summer monsoon (e.g., Yasunari 1979, 1980, 1981; Murakami 1984; Annamalai and Slingo 2001). ISOs at

Corresponding author: Hatsuki Fujinami, Hydrospheric Atmospheric Research Center, Nagoya, 464-8601, Japan.
E-mail: hatsuki@hyarc.nagoya-u.ac.jp

submonthly (6–25 days) timescales (e.g., Vincent et al. 1998) also occur over the region affected by the Asian summer monsoon (e.g., Krishnamurti and Bhalme 1976; Murakami 1976; Yasunari 1979; Krishnamurti and Ardanuy 1980; Chen and Chen 1993; Fukutomi and Yasunari 1999, 2002; Annamalai and Slingo 2001). These studies suggest that the effects of the submonthly oscillations on monsoon activity can be as important as the effects of 30–60-day oscillations.

Common features of the 10–20-day mode over the Asian summer monsoon region have been reported. Murakami (1976) used Indian Daily Weather Reports and upper-air observations from the summer of 1962 to show that a quasi-biweekly oscillation influences the active/break cycle of the monsoon over India. Krishnamurti and Bhalme (1976) analyzed nine monsoon elements and revealed a biweekly signal. Later, Krishnamurti and Ardanuy (1980) showed that monsoon breaks over India coincide with the arrival of a ridge in the 10–20-day westward propagating mode. Chen and Chen (1993) investigated the horizontal structure of 10–20-day ISOs in the Asian summer monsoon for the boreal summer of 1979. They found that the 10–20-day monsoon mode has a double-cell structure: one cell is centered between 15° and 20°N, and the second cell is over the equator. The two linked cells propagate westward along the Indian monsoon trough and along the equator, respectively. Fukutomi and Yasunari (1999) found prominent 10–25-day oscillations over the South China Sea during the early summer. Enhanced (suppressed) convective anomalies are associated with cyclonic (anticyclonic) circulation anomalies in the lower troposphere. These circulation anomalies propagate westward from east of the Philippines to the Arabian Sea.

Analyses of precipitation data yield conflicting results. Annamalai and Slingo (2001) used the ECMWF 15-year reanalysis and OLR data for 1979 to 1995 to produce a generalized view of the submonthly variability in summer (June through September), based on daily All-India monsoon rainfall (AIR). The power spectrum of the 17-year average daily AIR series has statistically significant peaks at both 12 and 16 days. The 10–20-day mode originates over the equatorial western Pacific, in association with westward-propagating Rossby waves. By contrast, Hartmann and Michelsen (1989) analyzed daily precipitation from Indian stations between 1901–70, and a 10–20-day mode is not statistically significant in the 200-day time series beginning on 10 April except over parts of northern India. They did show statistically significant peaks at 5–7-day and 40–50-day periods in the precipitation records. The data and analysis periods in the two studies differ, so a simple comparison is impossible. However, the inconsistency suggests that activity with submonthly timescales over India has variability at large interannual or longer timescales. Annamalai and Slingo (2001) show that the 30–60-day mode is strong during monsoon onset (early June) over India, whereas the 10–20-day mode is more pronounced after the monsoon is established (July–August). Careful attention is warranted for interpreting power spectra for long-term time series. Our study regards the 10–20-day variation as a robust feature of the Asian summer monsoon.

The southern part of the Tibetan Plateau is a major part of the Asian summer monsoon domain (Murakami and Matsumoto 1994). Remarkable diurnal variation in convection occurs over the plateau during the summer (e.g., Murakami 1983; Nitta and Sekine 1994; Yanai and Li 1994; Fujinami and Yasunari 2001). The convection depends strongly on thermally-driven regional-scale circulations induced by plateau topography (Ueno 1998; Kuwagata et al. 2001; Kurosaki and Kimura 2002). Nevertheless, few authors have investigated convective variability on submonthly timescales over the Tibetan Plateau. Nitta (1983) described intraseasonal variation with periods of 10–15 and ~30 days in total heating, precipitation, and relative vorticity in a case study for the summer of 1979 for the upper troposphere over the eastern Tibetan Plateau. Endo et al. (1994) used upper-air soundings from 1993 and showed that quasi-biweekly fluctuations in meteorological elements dominate over the central plateau after the onset of the summer monsoon. Fujinami and Yasunari (2001, hereafter FY01; 2002) showed fluctuations in the diurnal amplitude of summertime convection with periods of about 14 days and about 30 days over the plateau. ISOs greatly influence diurnal variability over the plateau.

ISOs also occur in the extratropics (e.g., Krishnamurti and Gadgil 1985; Hsu and Lin 1992; Kiladis and Weickmann 1992; Ambrizzi et al. 1995; Terao 1998, 1999). Quasi-stationary Rossby waves occur in the Asian subtropical jet during northern summer, with well-confined zonal wavenumbers 5–7 (Terao 1998, 1999). Spectral peaks have periods of 14 days and 30–45-days. Propagation routes correspond to a wave-guide for Rossby waves. FY01 discussed a possible relationship between ISOs in convection over the plateau and ISOs in the upper-level wave-like disturbances. Murakami (1981) investigated 12–20-day oscillations on the Asian subtropical jet over and around the Tibetan Plateau during northern winter. Plateau topography profoundly influences oscillation formation, propagation, and dissipation.

Although submonthly ISOs (SISOs) exist over midlatitudes and the region influenced by the Asian summer monsoon, SISOs near the Tibetan Plateau during the boreal summer have not been described precisely. Therefore, the objectives of this paper were: 1) to detail the evolution of convective activity and circulation fields in the 7–20-day band over and around the Tibetan Plateau during the summer and 2) to reveal a link between midlatitudes and the Asian monsoon, especially over India and the Bay of Bengal, during the transition from inactive to active convection over the plateau. The slightly broader temporal band used in this study is based on spectral analysis results.

Section 2 describes the data and analysis procedures, and includes results of time series analyses of equivalent blackbody temperature (Tbb) over the Tibetan Plateau. Section 3 describes large-scale mean fields of circulation and convection for years with enhanced submonthly convective variability over the plateau. Section 4 details composite relationships between 7–20-day convection over the plateau and large-scale OLR and circulation anomalies, and reveals a link in circulation changes between midlatitudes and the Asian monsoon region. Section 5 discusses the formation mechanisms for the wavetrain over the subtropical jet that links the convective signals between midlatitudes and the Asian monsoon. Section 6 contains concluding remarks.

2. Data and methods of analysis

2.1 Data

This study uses 3-hourly IR-Tbb data derived from a geostationary meteorological satellite (GMS). Tbb data are defined at each $1^\circ \times 1^\circ$ grid point. This relatively fine spatial and temporal resolution describes the convection over the plateau. Unfortunately, IR-Tbb data do not cover areas west of 80°E, so daily averaged interpolated outgoing longwave radiation (OLR) data produced by the National Oceanic and Atmospheric Administration (NOAA) Climatic Diagnostics Center (CDC) are also used as a proxy for large-scale convection (Liebmann and Smith 1996). Daily averaged National Center for Environmental Prediction (NCEP)/National Center for Atmospheric Research (NCAR) reanalysis data represent the large-scale circulation (Kalnay et al. 1996) from 1985 through 1998. Both OLR and reanalysis data are defined on global $2.5^\circ \times 2.5^\circ$ grids. Streamfunction (ψ) and velocity potential (χ) were calculated from the wind data using a spectral transform method with spherical harmonic R25 truncation.

2.2 Time-series analysis of Tbb

Figure 1 shows the horizontal distribution of the 14-year mean convective index (Ic) for July–August. The Ic is defined as $Ic = 250$–Tbb (K) if 250–Tbb is positive; $Ic = 0$ if 250–Tbb is negative. FY01 also used the 250 K thresh-

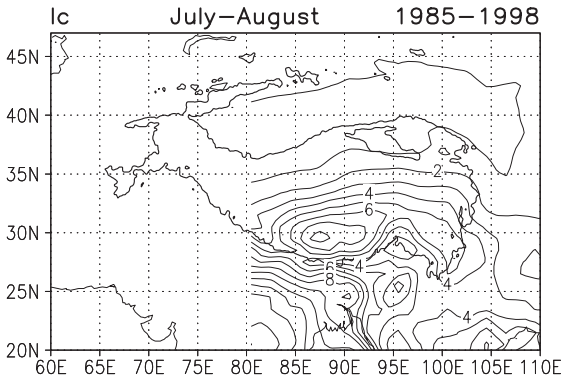

Fig. 1. 14-year averaged (1985–98) Ic for July–August (thin solid line). The contour interval for Ic is 1. The topographic contour for 3,000 m is also shown (thick solid line).

old to identify convective activity. Convective activity is most active during July–August, as shown in FY01. The region (28°–34°N, 85°–94°E) over the southern part of the plateau, where *Ic* shows a local maximum, is used to study convective fluctuations.

A spectral analysis using a fast Fourier transform (FFT) was used to detect the optimal frequency band of the fluctuations. The seasonal cycle was removed from the daily averaged Tbb data before applying the FFT by subtracting the first three harmonics of the annual cycle (about 120 days) at each grid point. Cosine tapering was applied to 10% of the time series at either end. FFT analyses used the detrended data averaged over the study region between June 1 and September 30 (122 days). A 3-point running mean in the frequency domain was applied to the raw spectra to reduce estimate errors.

Attention is focused on the SISO centered on the 14-day period. Figure 2 shows the interannual variation of the 11.6–16-day variance of Tbb, which helps to determine when a prominent SISO occurs over the plateau. There is a large quasi-biennial variation in the variance at this timescale. We use 1986, 1993, and 1998 to show typical SISO features near the Tibetan Plateau, because the variance is largest in those three years. Variance is also large in 1985, but because the 14-day period variability only occurred intermittently with large amplitude during July–August, that year was not used.

Figure 3-a shows both the 3-year averaged power spectrum of the daily Tbb anomalies for the study region and the red-noise spectrum and its 95% confidence level based on the red-noise model of Gilman et al. (1963) and Mitchell (1966). There is a pronounced peak at a period of about 14 days and the peak exceeds the 95% confidence level. By contrast, Fig. 3-b shows the mean for the other years (1985–98

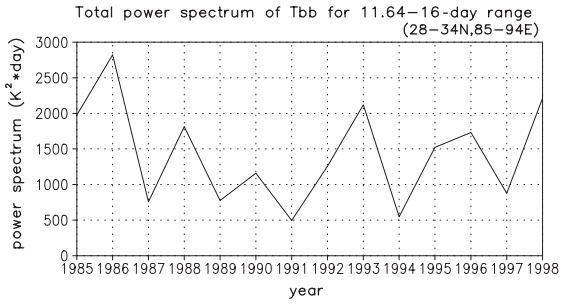

Fig. 2. The interannual variability of the total power spectrum of Tbb for timescales in the 11.64–16-day range over the base region (28°–34°N, 85°–94°E).

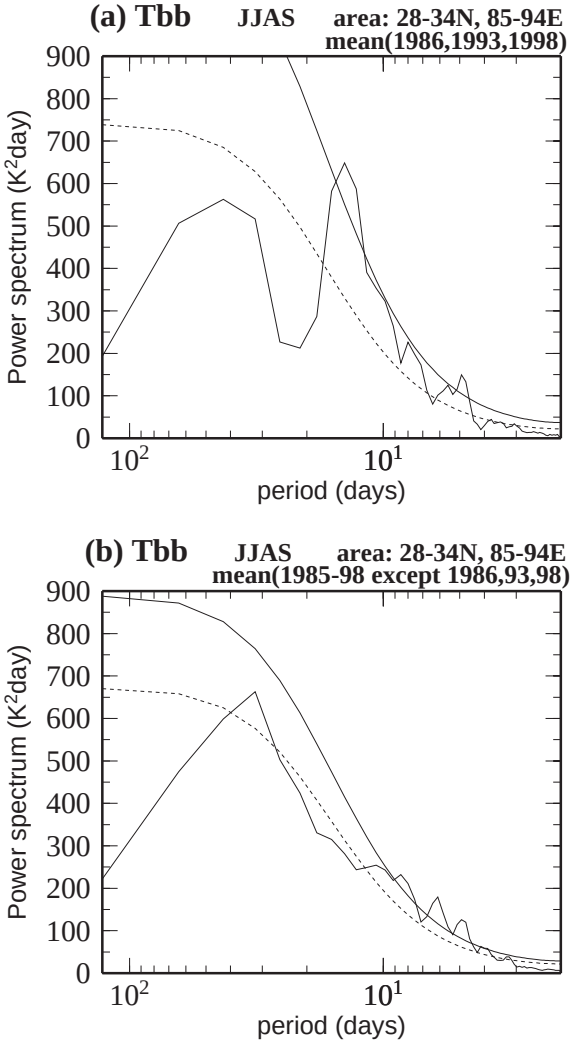

Fig. 3. Ensemble power spectra of area-averaged (base region: 28°–34°N, 85°–94°E) Tbb daily time series from June to September (122 days). (a) 3-year mean (1986, 1993, 1998); (b) 11-year mean (1985–1998 except 1986, 1993, 1998). A red-noise spectrum (dashed curve) and its 95% level of significance (solid curve) based on a lag-1 autocorrelation are also shown.

except 1986, 1993 and 1998); the 14-day variance blends into a red background spectrum. There is a peak at a period of about 30 days, but the peak fails to reach the confidence level. Therefore, this important period in intraseasonal convective variability has large interannual variability. Figure 3-a shows distinct spectral gaps at periods of about 7 and 20 days, so a 7–20-day band was chosen as the submonthly timescale for this study. The data were then temporally filtered using a Lanczos filter (Duchon 1979) to pass only variability in the selected period range. This band accounts for more than 45% of the total Tbb variance over the study region during July–August for the 3 years 1986, 1993, and 1998 (not shown) if seasonal cycles and diurnal variability are excluded. The region contains an action center of Tbb fluctuation at these timescales, and the study region is treated as a base region. A similar procedure was followed for other variables used in this study.

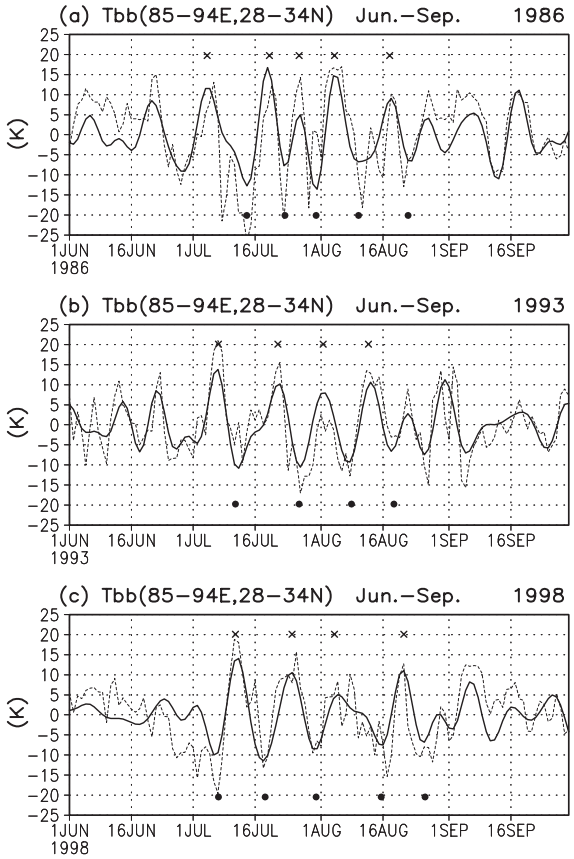

Fig. 4. Time series of detrended Tbb anomalies (dashed line) and 7–20-day filtered anomalies (solid line) averaged over the base region (28°–34°N, 85°–94°E). Closed circles and crosses denote selected active phases and inactive phases of convective activity for a composite analysis, respectively.

2.3 *Composite procedure*

Temporal variation in the circulation and large-scale convection associated with submonthly convective fluctuations over the Tibetan Plateau was examined using a time-composite technique. Figure 4 shows the detrended daily Tbb anomalies (dashed line) and the corresponding 7–20-day filtered anomalies (solid line) over the base region for the 3 years 1986, 1993, and 1998. Large amplitude 7–20-day oscillations appear continuously from July to August in each year. Dots and crosses respectively denote active and inactive convective events that exceed 1.0 standard deviation (5.6 K) except for two cases. Thirteen cycles were selected for the composite.

Eight phases comprise each cycle. Figure 5 shows the composite Tbb anomalies over the base region. Phases 3 and 7 correspond to the inactive and active extremes of convection.

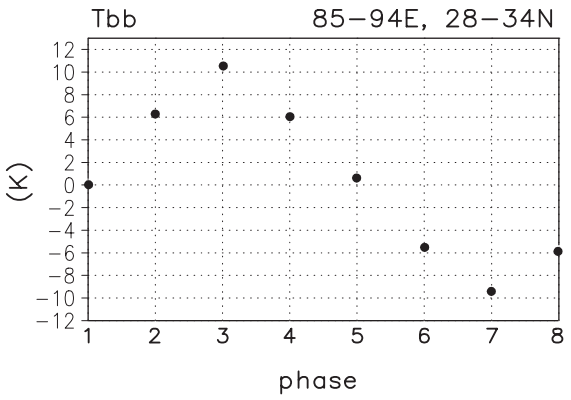

Fig. 5. Composite variability of the 7–20-day filtered Tbb anomalies averaged over the base region (28°–34°N, 85°–94°E).

Since the cycle period is about 14 days, the mean interval between phases is about 1.8 days. Composite fields were made for each phase. Each composite anomaly map was tested for statistical significance at the 95% level. Before the samples were averaged, composite maps for OLR and streamfunction anomalies for each year were made to verify similar spatial structures in each year.

3. Large-scale mean conditions

Figure 6 shows 3-year (1986, 1993, 1998) means for July–August of streamfunction and wind fields at; (a) 200 hPa, (b) 500 hPa, and (c) OLR and wind fields at 700 hPa. In Figs. 6-a and b, shading denotes positive values for the difference in zonal wind between the 3-year mean and the other years (1985–98 except 1986, 1993, and 1998) mean. Shading in Fig. 6-c denotes negative OLR differences. Closed circles denote that the difference is significant at the 95% confidence level. There is a large 200 hPa anticyclone (the Tibetan high) at 82°E with a ridge axis along 28°N (Fig. 6-a). The westerly Asian subtropical jet is at 40°N. Easterlies prevail south of 28°N. The zonal wind difference has a zonally tripole structure. There are positive anomalies along 30°N and negative anomalies along 15°N and 50°N from 40° to 150°E. Zonally-elongated positive (negative) anomalies at 30°N (50°N) suggest that the subtropical jet is at lower latitudes in the 3-year mean. Significant positive signals are also observed over the jet entrance region (around 45°N, 30°E). Enhanced submonthly variability over the Tibetan Plateau is strongly affected by changes in the atmospheric basic state over the midlatitudes. There are two anticyclones along 25°N at 500 hPa (Fig. 6-b). One is over Africa and the other is over the Pacific. The Tibetan Plateau is between these two anticyclones. A cyclonic circulation is centered near 20°N, 82°E over India and the Bay of Bengal. At 700 hPa, a monsoon trough is centered over northern India (Fig. 6-c). Enhanced convection (OLR < 220 W m^{-2}) occurred over India, the Bay of Bengal, the South China Sea, and the Tibetan Plateau. Active convective anomalies (shown as shading) spread zonally along 40°N; suppressed convective signals are along 20°N. Significant negative OLR anomalies extend from China to Japan and correspond to en-

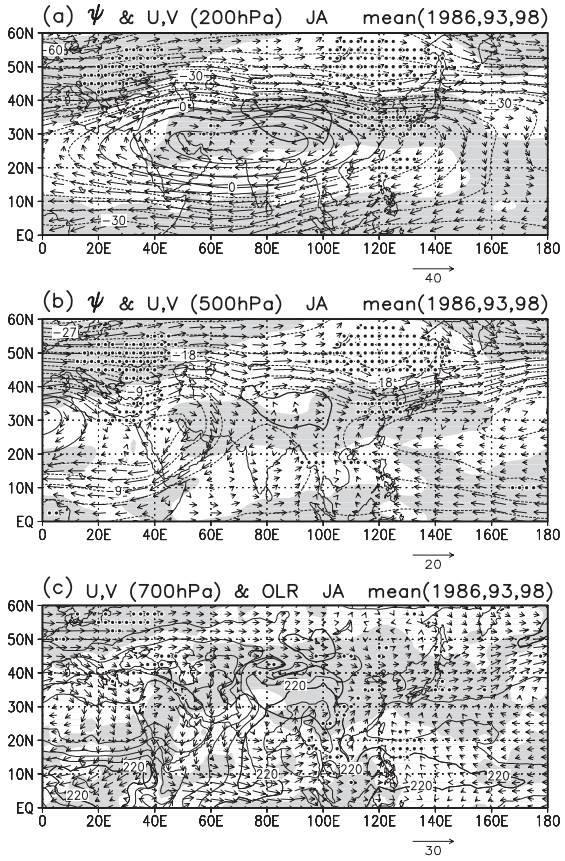

Fig. 6. Spatial distributions of the 3-year mean (1986, 1993, 1998) fields for July–August. (a) Streamfunction (ψ) and wind fields at 200 hPa. The contour interval is 6.0×10^6 m^2 s^{-1}. The difference between the 3-year averaged zonal wind and that averaged for the other years (1985–98 except 1986, 1993, 1998) is also shown. Positive anomalies are shaded. Closed circles indicate a significant difference at the 95% confidence level. The topographic contour for 3,000 m is also shown (thick solid line). (b) As in (a) but for 500 hPa. The contour interval is 3.0×10^6 m^2 s^{-1}. (c) OLR and wind fields at 700 hPa. The contour interval is 20 W m^{-2}. Shading denotes areas with negative OLR anomalies. The topographic contour for 1,500 m is also shown (thick solid line). The reference arrow is (a) 40, (b) 20, and (c) 30 m s^{-1}.

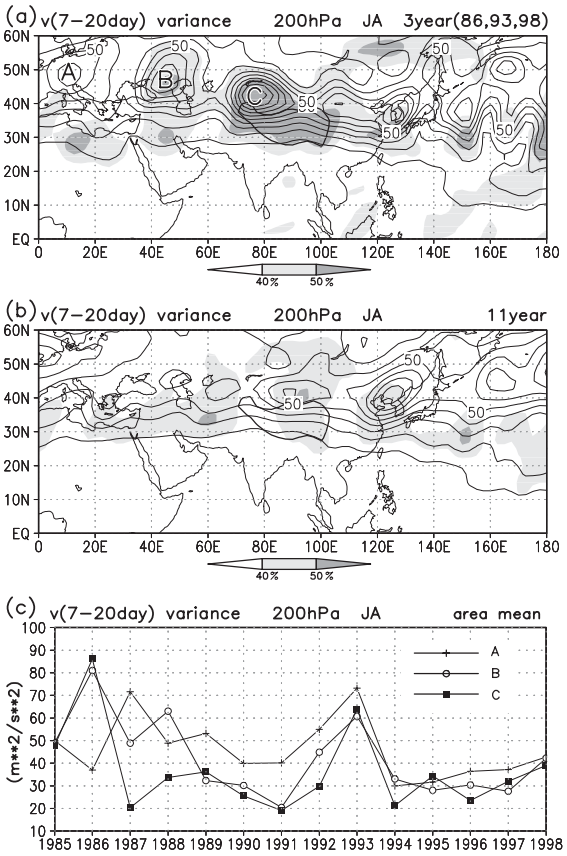

Fig. 7. (a) 3-year averaged (1986, 1993, 1998) 7–20-day filtered 200-hPa meridional wind variance for July–August. The contour interval is 10 m^2 s^{-2}. Shading represents the percent of the total variance (with the seasonal cycle removed) explained by the 7–20-day band. The thick solid line is the 3,000 m topographic contour. (b) As in (a) but for the years 1985–98, except 1986, 1993, and 1998. (c) Interannual variation of 7–20-day filtered 200-hPa meridional wind variance for July–August averaged over 5°–15°E, 40°–60°N (marked 'A' in (a), solid line with cross marks), 40°–50°E, 40°–60°N (marked 'B' in (a), solid line with open circles) and 70°–80°E, 30°–50°N (marked 'C' in (a), solid line with closed squares).

hanced convection in the subtropical (Baiu) frontal zone.

Convective fluctuations over the Tibetan Plateau with timescales of 7–20 days are strongly affected by waves with the same timescales in the Asian subtropical jet. Figure 7 shows 200-hPa meridional wind variance with timescales of 7–20 days during July–August. Shading denotes the percent of the total variance explained by the 7–20-day band (without the seasonal cycle). In the 3-year mean (Fig. 7-a), the variance field shows large values originating upstream from the plateau. Variance peaks occur at roughly regular intervals from 10 to 130°E, which suggests that the waves are zonally phase-locked. The 7–20-day variance accounts for more than half the total variance in the 3-year mean field over the plateau. By contrast (Fig. 7-b), in the other years, large variance occurs downstream from the plateau. A large variance is present over the three regions marked 'A', 'B' and 'C' in Fig. 7-a. The variation between the three regions has a nearly in-phase relationship (Fig. 7-c), suggesting dynamic linkage between the regions. Variance over region C strongly influences convective variability over the plateau; large values occur especially in 1986 and 1993. In 1998, although the values are not as large as in 1986 and 1993, the variance peak is over the same region.

The power spectrum of meridional wind time series over region C is shown in Fig. 8 to confirm the dominant period of the midlatitude waves. In the 3-year mean (Fig. 8-a), the spectrum has a significant peak at 16 days. Submonthly variability is pronounced in the upper-level midlatitude waves. Unlike the Tbb spectrum in Fig. 3-b, the meridional mean wind spectrum for the remaining years shows a spectral peak at 14 days (Fig. 8-b), although the peak fails to reach the confidence level by a narrow margin. The variance near 42°N, 90°E in Fig. 7-b, which is about 1,000 km east of Region C, has a significant peak with a 14-day period (not shown). The Asian subtropical jet and Tibetan high have vigorous submonthly intraseasonal variability during the boreal summer.

4. Spatial structure and temporal evolution

4.1 Convective activity

Figure 9 shows successive composite maps of the 7–20-day OLR anomalies from Phases 1 to 8. Open circles denote locally statistically significant grids at the 95% confidence level ac-

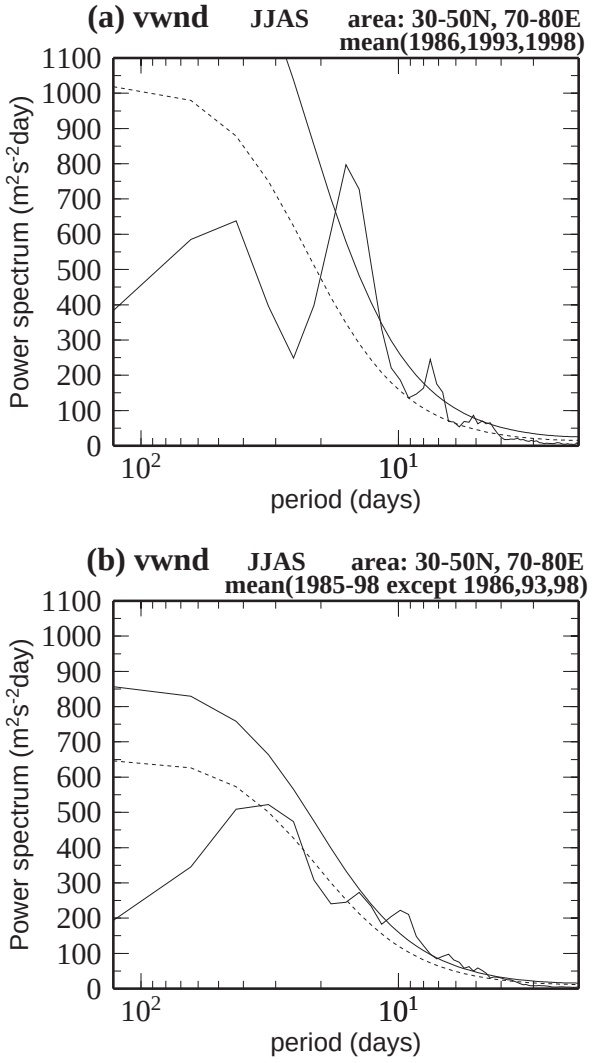

Fig. 8. As in Fig. 3, except for the area-averaged (70°–80°E, 30°–50°N) 200-hPa meridional wind time series.

cording to a standard *t*-test. Negative (positive) OLR anomalies indicate active (inactive) convective phases.

Phase 1 is characterized by an asymmetric east-west pattern around the plateau. Significant negative OLR anomalies occur over the eastern part of the Tibetan Plateau and around the Philippines, while positive anomalies extend from the westernmost region of the plateau to over India. Nitta (1983) noted the 14-day period in the out-of-phase precipitation relationship between central India and the eastern Tibetan Plateau. This relationship is also present in the OLR anomalies. The asymmetric east-west pattern changes into an asymmetric north-south (or dipole) pattern between the Tibetan Plateau and the Bay of Bengal as Phase 1 evolves into Phase 3.

The suppressed area of convection over the plateau moves eastward from Phase 3 to 6. During Phase 4, negative anomalies blossom over the western flank of the plateau, and the negative OLR anomalies over the Bay of Bengal migrate westward to the Indian subcontinent. By Phase 5, the asymmetric north-south anomaly pattern again becomes an asymmetric east-west pattern, but its sign is opposite that in Phase 1. Phase 7 is nearly opposite to Phase 3. From Phase 7 to 8, negative OLR anomalies spread eastward over the plateau, while there are positive anomalies over the Bay of Bengal and western part of the plateau. Then, the structure returns to Phase 1.

This Phase sequence describes a clockwise rotation of OLR anomalies around 28°N, 90°E over and around the Tibetan Plateau, including Indochina, the Bay of Bengal, and India. Yasunari (1979) showed a phase-lag relation for a 10–20-day mode of cloudiness with three reference areas, which are located over central India, Malaysia, and the eastern Tibetan Plateau. The phase differences in our study agree with that result.

Significant signals also occur near the Philippines, which have an out-of-phase relation to the Bay of Bengal, India, and the western Tibetan Plateau, and are in phase with the eastern Tibetan Plateau. Negative OLR anomalies develop around the Philippines and then move westward, decaying slightly as they move. The negative anomalies expand rapidly as they reach the head of the Bay of Bengal. These anomalies then propagate westward to India. These active convective signals are accompanied by lower tropospheric cyclonic anomalies (not shown). Krishnamurti and Ardanuy (1980) and Chen and Chen (1993) show a similar westward propagating mode. Heavy precipitation over India during the Asian summer monsoon accompanies monsoon lows or monsoon depressions that move westward from the Bay of Bengal. Yasunari (1981) noted that these monsoon depressions appear in phase with negative geopotential anomalies with quasi-biweekly periods as well as 40-day

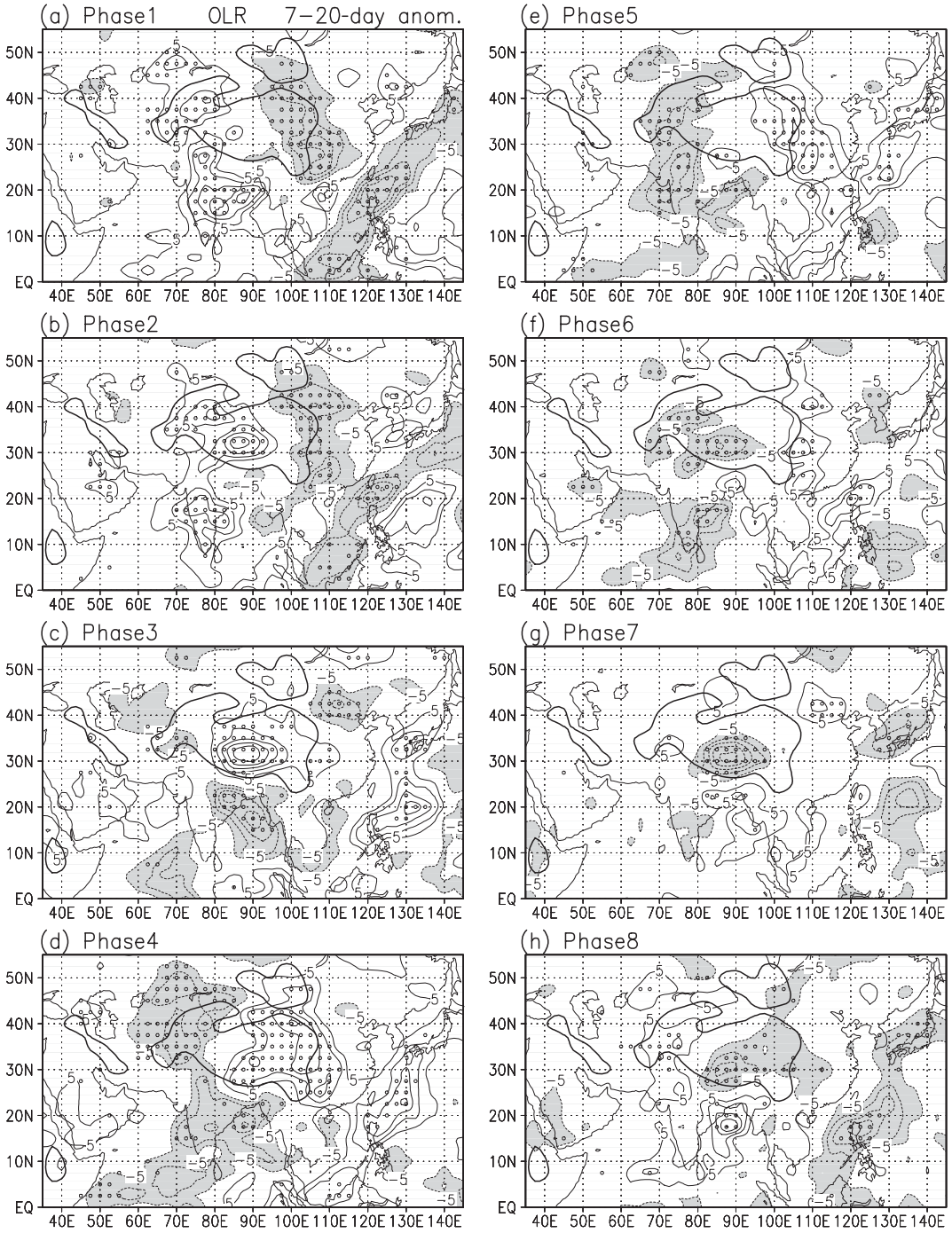

Fig. 9. Spatial distribution of composite OLR anomalies in the 7–20-day band from Phase 1 (a) through Phase 8 (h). The contour interval is 5 W m^{-2}. The zero contour is not plotted. OLR anomalies less than -5 W m^{-2} are shaded. Open circles indicate locally statistically significant grids. The 1,500 m topographic contour is shown as a thick solid line.

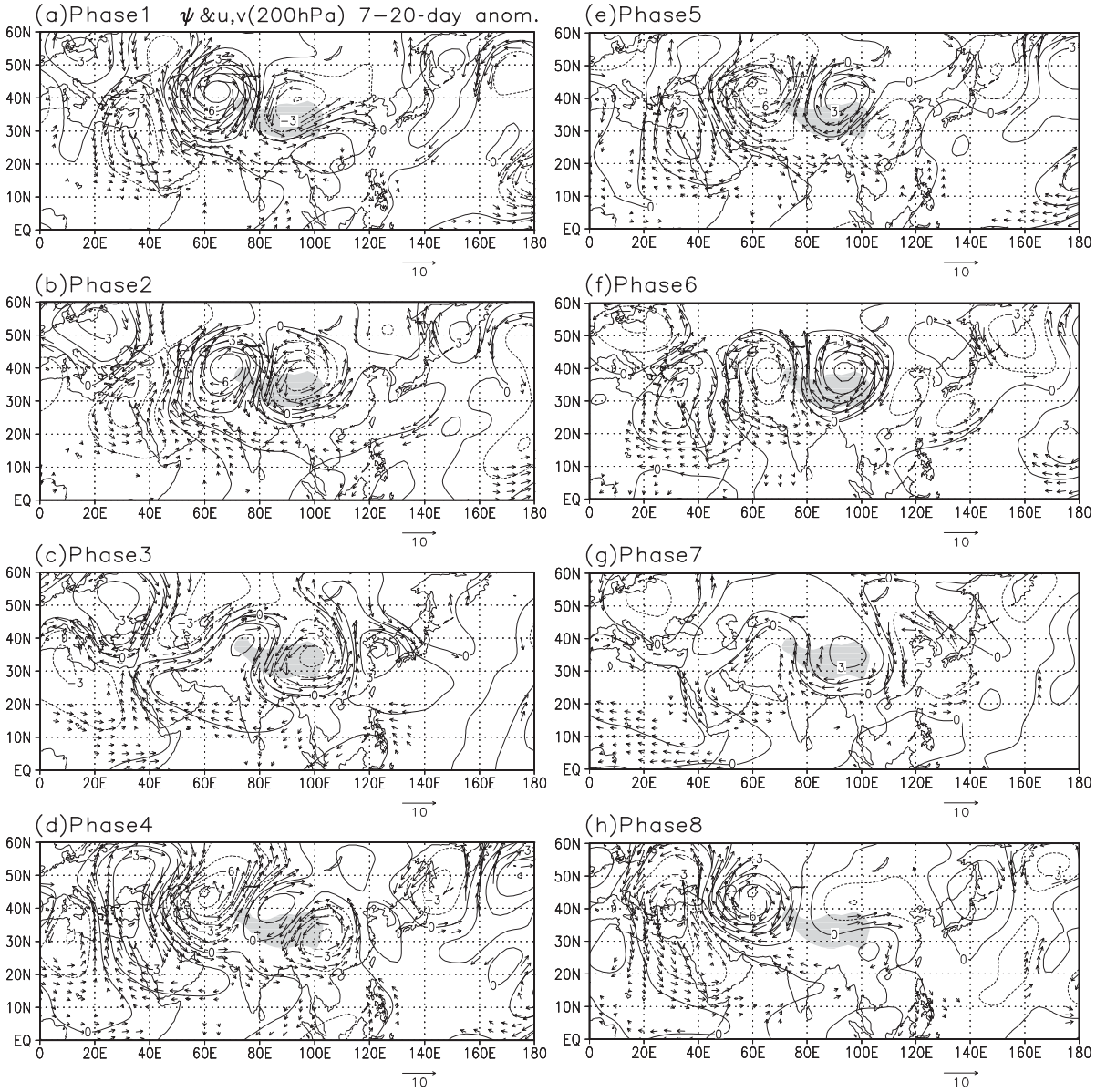

Fig. 10. Spatial distribution of composite streamfunction (ψ_{200}) and locally statistically significant wind vector anomalies in the 7–20-day band at 200 hPa from Phase 1 (a) through Phase 8 (h). The contour interval is 1.5×10^6 m^2 s^{-1}. The unit vector is 10 m s^{-1}. Shading denotes the Tibetan Plateau.

periods. The southern portion of the clockwise rotation includes the monsoon depressions. Other major components of the clockwise rotation extend over the Tibetan Plateau. The next focus is on formation processes for OLR anomalies along the northern part of the clockwise rotation.

4.2 Upper-level atmospheric circulation

Figure 10 shows the evolution of streamfunction (ψ_{200}) and wind vector anomalies at 200 hPa from Phase 1 to 8. Wind vectors are plotted where either the u or v component exceeds the 95% local confidence level.

A well-developed wave train extends from

North Africa to far-east Asia associated with 7–20-day convection over the plateau. Anomalies also overspread nearly the entire Tibetan high. An anomalous anticyclone (positive ψ_{200} anomaly), centered near 42°N, 65°E, develops to the west of the plateau from Phase 1 to Phase 2 as part of the wave train. Anomalous northerlies lie along the eastern fringe of this anticyclone, accompanied by suppressed convection. There is an anomalous cyclone (negative ψ_{200} anomaly) over the plateau. This cyclone shows a slight southwest-northeast tilt with a southwesterly flow on its eastward flank, where there is also active convection. There are also significant easterly anomalies near 18°N from 60° to 100°E associated with strengthened easterlies. In Phase 3, northerly anomalies dominate over the base region only. South of 30°N, an anticyclonic anomaly over western Tibet and easterly anomalies to its south both move westward. The westward-propagating anticyclonic anomaly and a second anticyclonic anomaly centered near 50°N, 30°E merge into a single north-south elongated anticyclonic anomaly along 35°E by Phase 4.

Structures change dramatically upstream from the wave train from Phase 3 to 4. ψ_{200} anomalies acquire a sign opposite to those at Phase 1 and 2. A cyclonic anomaly develops rapidly near 43°N, 60°E, west of the plateau, and active convection strengthens ahead of this trough. From India to Indochina along 20°N, wind anomalies reverse and westerly anomalies become prominent. At Phase 5, the ψ_{200} anomalies are the inverse of those in Phase 1 as the spatial relationship between the Tibetan Plateau and anomalous trough and ridge reverses. Figs. 9-a and e show that the east-west asymmetric pattern of OLR anomalies has the opposite sign between the two phases. In Phase 6, local strengthening of the Tibetan high is manifest as a positive ψ_{200} anomaly over the plateau maximizing before the peak in convection over the plateau. Convective activity peaks after the ridge strength peaks. At submonthly timescales, waves do not amplify in response to heating by convection over the plateau. Rather, midlatitude waves force the convective activity over the plateau.

Figure 11 shows a composite phase-longitude cross-section of the ψ_{200} anomalies averaged between 30° and 45°N to show the characteristics of the waves more clearly. A quasi-standing wave pattern is obvious, with a zonal wavenumber of about 7. These waves slowly move eastward with an average eastward phase speed of about 4 m s^{-1}, as indicated by the dashed arrow. By contrast, wavelike structures and successive downstream development of new centers of action occur, as denoted by the solid arrow. This phenomenon is generally interpreted as Rossby wave energy dispersion on the sphere (Blackmon et al. 1984) and is clearly distinct from the phase propagation associated with the higher-frequency transients (baroclinic waves). Ambrizzi et al. (1995) and Terao (1998) describe similar downstream developments along the Asian jet during northern summer, which they interpreted as evidence of Rossby wave dispersion along a wave-guide for Rossby waves. The wave characteristics in those studies are similar to wave characteristics in this study, so an interpretation similar to the previous studies is applicable here. A composite group velocity of about 22 m s^{-1} can be estimated from the slope of the solid arrow. Murakami (1981) has shown that in the northern winter, 200-hPa 12–20-day vorticity perturbations have prominent standing oscillations superimposed on modes propagating slowly eastward (at about 4 m s^{-1}) in the subtropical jet (45 m s^{-1}) south of the Tibetan Plateau. FY01 shows a similar standing oscillation in spatial structures around the plateau during March–April (their Fig. 10). The standing

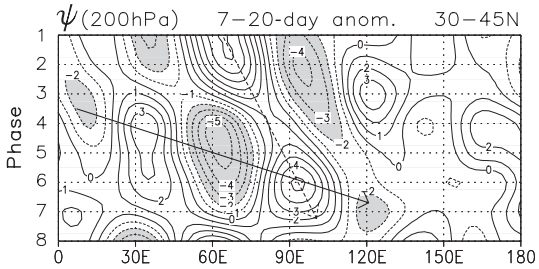

Fig. 11. Composite phase-longitude section of the 7–20-day streamfunction anomalies (ψ_{200}) at 200 hPa averaged between 30° and 45°N. The contour interval is 1×10^6 m^2 s^{-1}. ψ_{200} anomalies less than -2×10^6 m^2 s^{-1} are shaded. See the text for the explanation of the arrows.

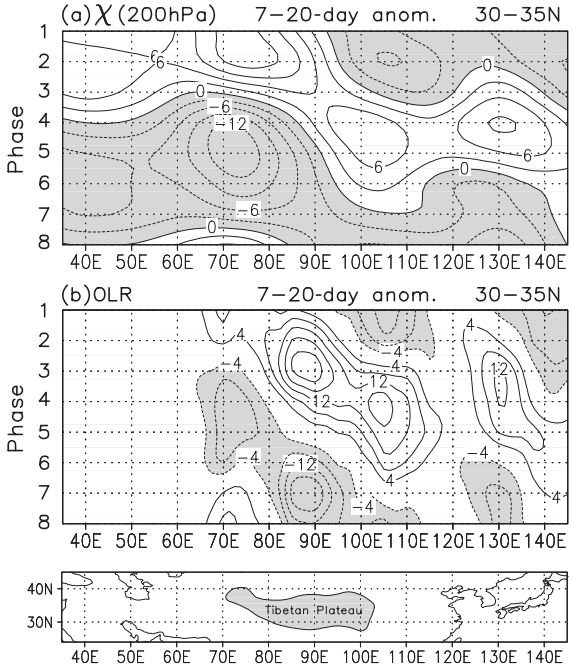

Fig. 12. Composite phase-longitude sections of the 7–20-day anomalies between 30° and 35°N. (a) Velocity potential (χ_{200}) anomalies at 200 hPa. The contour interval is 3×10^5 m^2 s^{-1}; negative (divergent) anomalies are shaded. (b) OLR anomalies. The contour interval is 4 W m^{-2}. Anomalies less than -4 W m^{-2} are shaded. A map with a different aspect ratio is shown in the bottom figure.

oscillation is associated with marked zonal wind anomalies over the plateau in winter and spring and meridional wind anomalies in summer.

Upper-level divergence is associated with the submonthly convective variation and fluctuates with timescales of 7–20-days over and around the plateau. Figure 12-a shows a phase-longitude section of composite velocity potential (χ_{200}) anomalies at 200 hPa averaged between 30° and 35°N. The velocity potential represents only large-scale divergence fields because the inverse Laplacian operation smoothes smaller scale features. Negative anomalies represent divergence and regions of rising motion. Figure 12-b shows the same region as Fig. 12-a, but shows OLR anomalies. For convenience, the corresponding geographic map is shown at the bottom. Regions of upper-air divergence (convergence) agree with negative (positive) OLR anomalies to the east of 65°E. Significant OLR anomalies do not appear west of 65°E, suggesting that the relationship between midlatitude waves and convective activity is made visible by a divergent circulation to the east of 65°E.

From Phase 8 to 2, upper-air convergence occurs where convection is suppressed over the western flank of the plateau. Upper-air divergence and active convection occur over the eastern flank of the plateau. The upper-level convergence moves eastward from Phase 2 to 4, and becomes established over the eastern flank of the plateau in Phase 5. In Phase 3, convergence implies large-scale subsidence over the plateau. From Phase 4 to 6, divergence develops over the western flank of the plateau near 72°E, as a cyclonic anomaly approaches from the west and strengthens near 65°E. The divergence then moves eastward from Phase 6 to 8 with an active convection signal. Note that the divergent anomalies are already established over the western Tibetan Plateau and influence the base region before the active convection over the base region. Upper-level divergent anomalies probably induce subsequent active convective anomalies.

Figure 13 shows composites of the total circulation field (left) and velocity potential and divergent wind anomalies (right) at 200 hPa from Phase 2 to 4. Positive and negative ψ_{200} anomalies in Fig. 10-b, c, d correspond to the ridge and trough, respectively, in the total field. The center of the Tibetan high during Phase 2 is near 28°N, 70°E (Fig. 13-a). There is an asymmetric east-west pattern of χ_{200} anomalies centered near 90°E between 10° and 50°N (Fig. 13-d) that corresponds to the OLR anomalies in Fig. 9-b. Around India, easterly divergent wind anomalies contribute to the easterly anomalies present in Fig. 10-b. Convergent fields dominate Phase 3 over the plateau (Fig. 13-e), reflecting subsidence that suppresses convection behind the deep trough. As enhanced convection migrates westward to the head of the Bay of Bengal, an anomalous ascending branch develops there. An asymmetric east-west pattern of χ_{200} anomalies occurs at Phase 4 (Fig. 13-f). Divergence becomes prominent over the western flank of the plateau where southwesterlies cross over the plateau ahead of a deepening

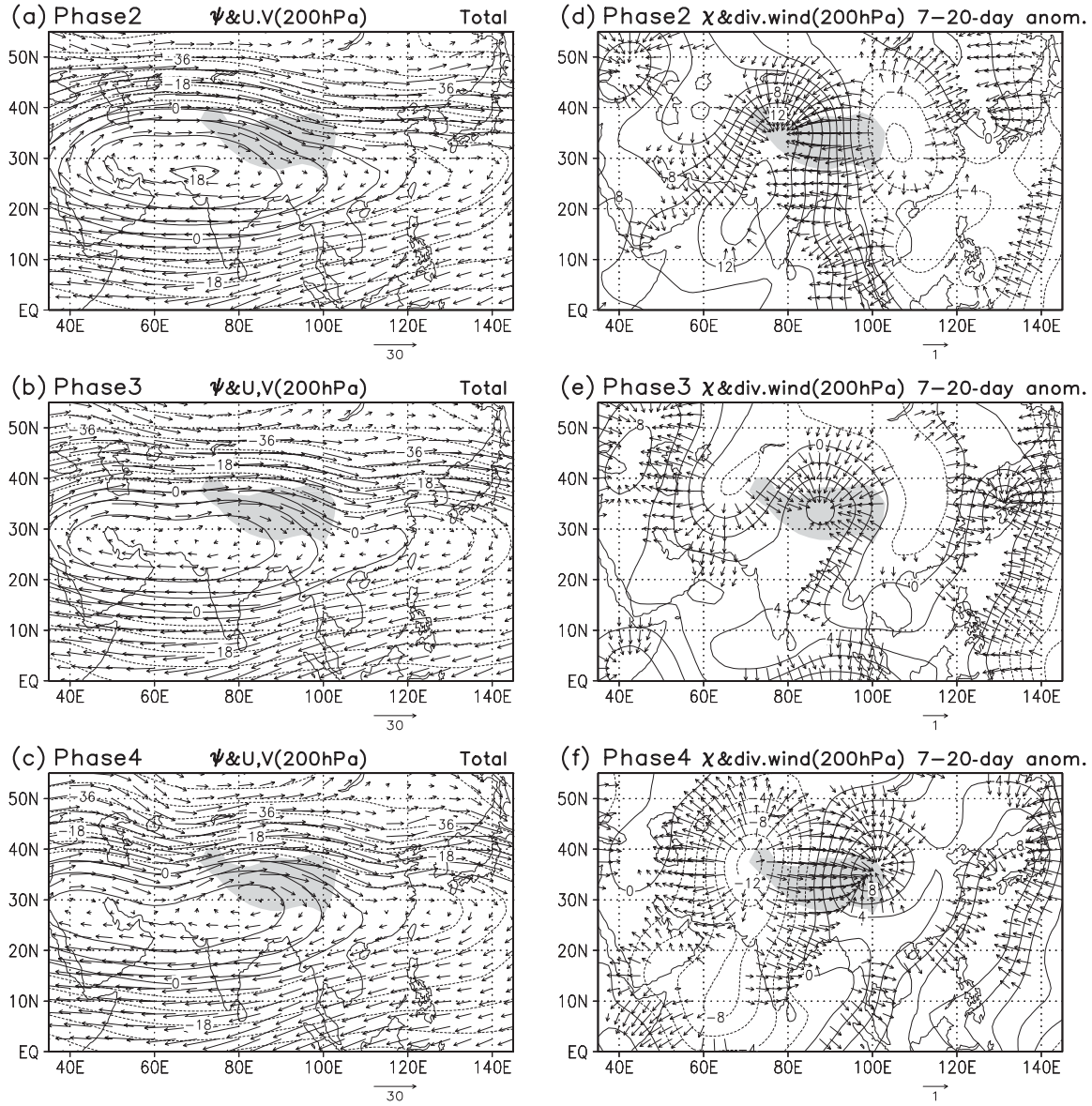

Fig. 13. Composite of (a–c) total 200-hPa streamfunction (ψ_{200T}) and wind fields; (d–f) 200-hPa velocity potential (χ_{200}) and locally statistically divergent wind anomalies in the 7–20-day band from Phase 2 to 4. The contour interval is (a–c) 6.0×10^6 m^2 s^{-1} and (d–f) 2.0×10^5 m^2 s^{-1}. The unit vector is (a–c) 30 m s^{-1} and (d–f) 1 m s^{-1}. Shading denotes the Tibetan Plateau.

trough (Fig. 13-c). Negative OLR anomalies over the western flank of the plateau is induced by forced ascent over the plateau barrier. Convergence over the eastern Tibetan Plateau forces subsidence. These sequences suggest that the midlatitudes and Asian monsoon region around the plateau interact through anomalous vertical circulations. Murakami (1981) has revealed that in winter, velocity potential fields at 200 hPa are greatly enhanced by topographic effects of the plateau, which tends to reduce the eastward vorticity advection by the strong westerly flow. A plateau-induced dynamic effect also influences the characteristics of the circulation fields around the plateau in summer.

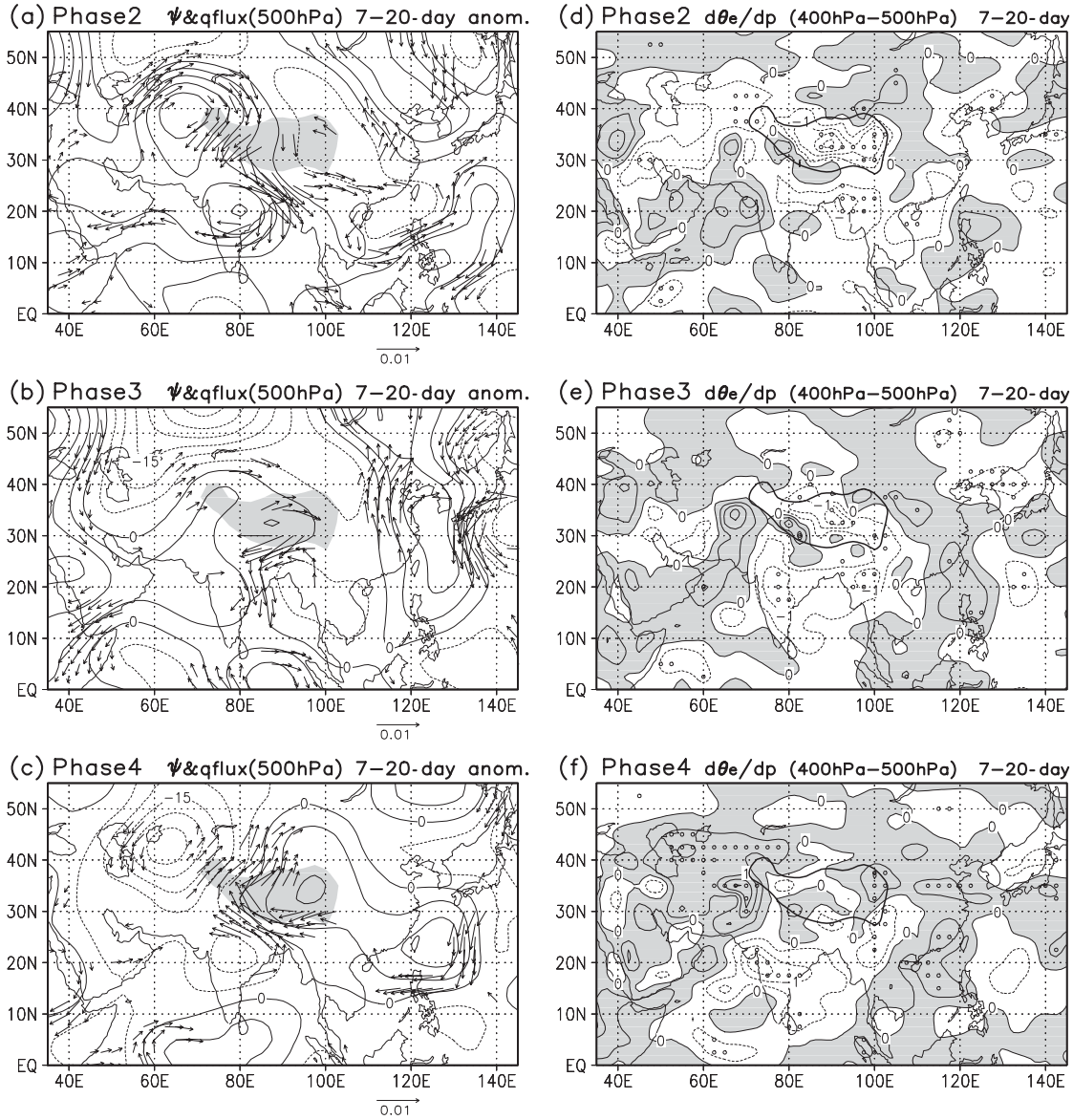

Fig. 14. Composite of (a–c) the 500-hPa streamfunction (ψ_{500}) and locally statistically significant moisture flux vector anomalies; (d–f) potential instability (θ_e/dp) anomalies from Phase 2 to 4. Potential instability is defined by the difference in θ_e between 400 and 500 hPa. The contour interval is (a–c) 5.0×10^5 m^2 s^{-1} and (d–f) 0.5 K $\cdot$ 100 hPa^{-1}. (a–c) A unit vector is 0.01 g g^{-1} m s^{-1}. Shading denotes the Tibetan Plateau. (d–f) Positive (unstable) anomalies are shaded. Open circles indicate locally statistically significant grids.

4.3 A link between the midlatitudes and the Asian monsoon region

Circulation fields in the lower troposphere influence convection. Figure 14 shows streamfunction (ψ_{500}) and the statistically significant moisture flux vector anomalies at 500 hPa (left) and the vertical gradient of equivalent potential temperature (θ_e, calculated as in Bolton (1980)) between 400 and 500 hPa (right) for Phase 2 through Phase 4. 500 hPa is the lowest NCEP/NCAR standard reanalysis pressure level above the plateau.

Phase 2 ψ_{500} anomalies have an asymmetric east-west pattern centered along 90°E between

10° and 50°N (Fig. 14-a). There is an anticyclonic circulation near 40°N, 65°E, similar to the location at 200 hPa (Fig. 10-b). Therefore, to the north of 30°N, except just over the plateau, the waves are nearly barotropic. A second positive ψ_{500} center is over India. There are northerly wind anomalies over the plateau. Northerlies also dominate over the plateau from 500 through 100 hPa in the total wind fields (not shown), moving a dry, cold air mass over the plateau. The vertical stratification is the most stable over the plateau in this phase (Fig. 14-d) and cloud development is inhibited by entraining or mixing of dry environmental air. Consequently, convective activity decreases. In Phase 3 (Fig. 14-b), a positive ψ_{500} center is over the plateau and comparison of ψ anomalies at 200 hPa (Fig. 10-c) suggests that a baroclinic structure is more prominent over the plateau. The anticyclonic anomalies suggest a strengthening of divergent flow at this level. The dryness, upper-level subsidence, and divergent flow in the lower troposphere combine to greatly suppress convection over the plateau.

The Phase 4 circulation pattern has approximately reversed Phase 2. The negative ψ_{500} anomaly at 20°N, 120°E in Phase 2 moves westward and reaches the Indian subcontinent in Phase 4 with active convection anomalies. Simultaneously, a second negative ψ_{500} anomaly develops west of the plateau, corresponding to a deepening of the upper-level trough (Fig. 10-d). This east-west pattern of ψ_{500} anomalies induces anomalous southerlies towards the plateau, which transports warm, humid air in the lower atmosphere. The lower atmosphere becomes convectively unstable over the plateau during this phase (Fig. 14-f). During Phases 5 and 6, the east-west pressure gradient strengthens. The most unstable conditions for moist convection appear over the base region during Phase 6 (not shown).

From Phase 2 to 4, negative ψ_{700} anomalies propagate westward from the Philippines to India in a manner similar to Figs. 14-a, b and c (not shown), and this propagation corresponds to a deepening of the monsoon trough over India in the total field.

Figure 15 shows composites of the total streamfunction at (a) 200, (b) 500, and (c) 700 hPa in Phase 5 to highlight the enhancement of the southerly moisture flow toward the plateau. Figure 15-a shows wind vectors and Figs. 15-b and c show moisture flux at each level. The upper-level trough deepens to the

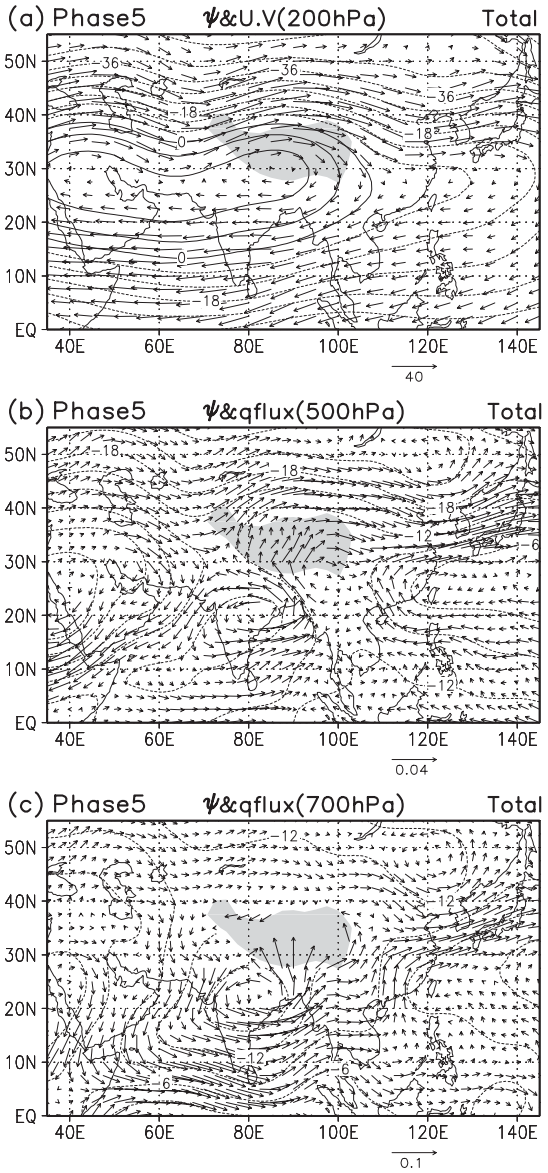

Fig. 15. (a) Total streamfunction and wind vectors at 200 hPa for Phase 5. As in (a) except for the moisture flux vector at (b) 500 and (c) 700 hPa. The contour interval is (a) 6.0×10^6 m^2 s^{-1} and (b), (c) 3.0×10^6 m^2 s^{-1}. The unit vector is (a) 40 m s^{-1}, (b) 0.04 g g^{-1} m s^{-1}, and (c) 0.1 g g^{-1} m s^{-1}. Shading denotes the Tibetan Plateau.

west of the plateau, and the ridge strengthens over the plateau. There is a deep trough at 500 hPa from 50°N, 65°E to 10°N, 80°E, and moisture flow toward the plateau is clearly observed to the east of it; this flow moistens the lower atmosphere over the plateau. At 700 hPa, as the monsoon trough deepens, moisture transport toward the plateau strengthens to the east of the trough. There is significant moisture transport toward the plateau between the lower and middle troposphere.

The Phase 7 circulation features are nearly identical to those in Figs. 12-a and 13-a in FY01, which are composites of circulation fields at 200 and 500 hPa for the active convective phase over the plateau in summer. Strengthening of the low-level cyclonic circulation enhances low-level convergence, although the southerly moisture inflow is reduced over the base region. The specific humidity at 500 hPa reaches its maximum because of the increase in precipitation. The antecedent moistening and convergence at low levels induces a convective maximum over the plateau.

5. Discussion

Convective variability of about 14-day period over the base region has large interannual variability (Fig. 2). The variance peak northwest of the plateau (around Region C in Fig. 7-a) reflects an alternation between southerly and northerly winds that import moist and dry air masses, respectively, over the base region and cause the large amplitude convective fluctuation in the 3 years (1986, 1993, 1998). By contrast, the variance peak around 42°N, 87°E in the other years is north of the plateau (Fig. 7-b) and is about 1,000 km east compared to Region C. In 1989, 1991, and 1997, ~14-day convective fluctuations are weak over the base region (Fig. 2). Although the dominant meridional wind period is ~14 days around 42°N, 87°E in these years, convection fluctuates with 9-, 7-, and 6-day periods over the base region (not shown). In 1997, the 40-day period was also dominant. These periods correspond to the timescales of the northerly (or dry air) intrusions into the base region. In 1987, 1990, and 1994, the ~14-day convective fluctuations are also weak because wave activity with 14-day timescales is suppressed along the jet near the plateau (not shown). In any case, the predominant periods in convection over the plateau are closely related to the variability of the Asian subtropical jet. An interannual change in the spatial relationship between the waves and plateau may vary the dominant periods of convective variability because of a shift in the meridional wind variance maximum.

Interannual variation in the basic atmospheric state is also likely to control the variation in the dominant periods for convective fluctuations. The Asian subtropical jet is displaced to lower latitudes in the 3-year mean fields (Fig. 6-a), indicating that the circulation around the plateau is sensitive to the influence of the midlatitude waves. Note that the zonal wavenumber 7 scale (about 5,000 km in wave length at 40°N) is almost the same zonal width as the Tibetan Plateau. The 7–20-day wave fluctuations may be amplified by wave-plateau interaction through a resonance-like phenomenon.

This diagnostic study revealed that a well-developed wave train extending from North Africa to far-east Asia along the Asian subtropical jet is associated with convective fluctuations over the Tibetan Plateau. Fukutomi and Yasunari (1999) showed that a wave train grows in both the lower and upper level atmosphere associated with submonthly convective fluctuations over the South China Sea. The wave growth is a Rossby mode response to anomalous heating (or cooling). However, significant submonthly-scale convective anomalies upstream from the midlatitude waves are not observed. This implies that the wave variability in Fig. 10 is induced by an internal unstable dynamic mode. Using a numerical simulation of a large-amplitude anticyclone forced by a localized mass source on a Beta plane, Hsu and Plumb (2000) showed that anticyclones are shed westward periodically due to instability. Popovic and Plumb (2001) used NCEP/NCAR reanalysis data for the period from 1987 to 1990 and confirmed the presence of westward-migrating anticyclones that detach from the main Tibetan High a few times each summer. Figure 10 for Phase 3 to 4 shows an anticyclonic anomaly south of 30°N over western Tibet moving westward. The anticyclone approached 40°E at Phase 4. This wave variation may be induced dynamically by an unstable mode in the large-scale circulation fields. Re-

cently, Enomoto et al. (2003) described a quasi-stationary Rossby wave along the Asian jet in August and called the waves "the Silk Road pattern". They proposed that localized mid-tropospheric descent over the eastern Mediterranean Sea and the Aral Sea is enhanced through the monsoon-desert mechanism, and associated upper-tropospheric convergence acts as a wave source near the jet entrance.

The clockwise rotation of convective signals implies that dynamic interactions exist between the midlatitudes and Asian summer monsoon. This study did not investigate the dynamic aspects of the interactions in detail; nevertheless, it is possible to show linkages in atmospheric circulation changes between the two regions. That is, simultaneous changes to the circulation fields west of the plateau and over India enhance convective activity over the plateau. A second linkage occurs north of the Philippines. Figure 10-g shows cyclonic upper air anomalies around 35°N, 125°E and extending to the Philippines in Phase 7. This cyclonic circulation is above mid- and lower-tropospheric cyclonic anomalies (not shown), which suggests barotropic enhancement of the cyclonic circulation. The cyclonic anomalies denote a weakening of the easternmost region of the Tibetan high in the upper troposphere, and the westernmost region of the subtropical high in the middle and lower troposphere. Subsequently, upper-air cyclonic anomalies weaken as cyclonic anomalies develop around the Philippines in the lower and middle troposphere coupled with an active convection signal in Phase 8. This sequence suggests that the SISO of the midlatitude waves initiates a SISO in the circulation and convection north of the Philippines. Enomoto et al. (2003) hypothesized that the equivalent barotropic structure of the Bonin (Ogasawara) high near Japan in summer results from the propagation of stationary Rossby waves along the Asian subtropical jet. A similar process may influence changes in circulation anomalies around the Philippines.

Figure 16 shows the difference in 7–20-day OLR variance between the 3-year mean and the other years mean during July–August. Positive anomalies extend over the base region and over other Asian monsoon regions as well. Submonthly variability increased over midlatitudes and the Asian monsoon regions in the 3 years. The upper-level Asian subtropical jet is displaced to lower latitudes in the 3-year mean fields. Further statistical and dynamic studies will determine how this displacement facilitates extratropical-subtropical interaction on submonthly timescales.

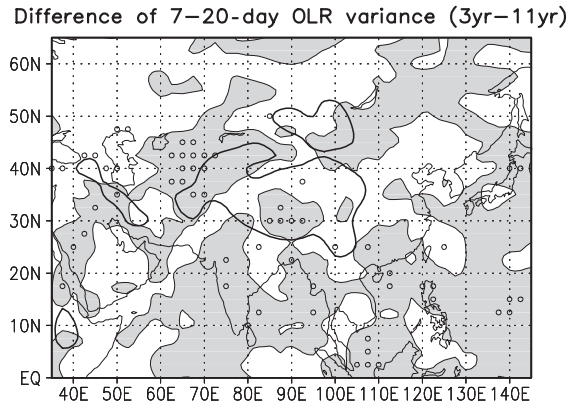

Fig. 16. Difference in the 7–20-day OLR variance between the 3-year (1986, 1993, 1998) and 11-year means (1985–1998 except 1986, 1993, 1998) for July–August. Positive areas are shaded. Open circles indicate locally statistically significant grids in the difference. The 1500-m topographic contour is shown as a thick solid line.

6. Concluding remarks

This paper examined the submonthly (7–20-day timescales) intraseasonal oscillation (SISO) of convective activity over the Tibetan Plateau and the associated large-scale convective activity and atmospheric circulations over and around the plateau during the mature phase of the Asian summer monsoon (July–August). A diagnostic study examined the three years when prominent submonthly convective variability was observed over the plateau. Relationships between midlatitudes and the Asian summer monsoon region were identified and are summarized as follows.

1) The variation in convection over the southern part of the plateau (the base region) with ~14-day periods shows large interannual variation. The variance is prominent especially in 1986, 1993, and 1998. Convective fluctuations with a timescale of 7–20 days account for more than 45% of the total variance during

July–August in the 3-year mean field over the base region.

2) Climatologically, areas of the Asian subtropical jet and Tibetan high near the plateau have vigorous submonthly intraseasonal variability during the boreal summer. In 1986, 1993, and 1998, the 7–20-day meridional wind variance fields have large values upstream from the plateau with a peak northwest of the plateau. In addition, the upper-level Asian subtropical jet is displaced to lower latitudes.

3) The submonthly convective anomalies show a clockwise rotation around 28°N, 90°E over and around the Tibetan Plateau, including Indochina, the Bay of Bengal, and India. Other significant anomalies appear near the Philippines and South China Sea. The southern track of the clockwise rotation includes westward moving monsoon depressions, and the northern track is induced by waves on the Asian subtropical jet.

4) A well-developed wave train extends from North Africa to far-east Asia along the Asian subtropical jet. The wave train is associated with submonthly convective fluctuations over the plateau. The waves have quasi-stationary behavior and a Rossby wave-like structure with a wavenumber of approximately 7. The waves also have a slow eastward phase speed. Circulation anomalies are observed over all of the Tibetan high.

5) Before convection minimizes over the plateau, an upper-air ridge develops to the west of the plateau as part of the wave train. The ridge induces northeasterly flow that moves dry, cold air over the plateau. Suppressed convection over the plateau results from antecedent drying in the troposphere, strengthening of upper-level subsidence, and low-level divergence.

6) Before convection maximizes over the plateau, an upper-level trough develops and deepens to the west of the plateau. Southwesterly flow ahead of the trough induces forced ascent (descent) over the western (eastern) flank of the plateau with active (suppressed) convection, causing an asymmetric east-west pattern in convection.

7) As the trough deepens to the west of the plateau, a cyclonic circulation also forms over India in the lower through middle troposphere. The enhanced trough forces a southerly moist flow in the lower atmosphere over the plateau. The moistening helps create a convectively unstable condition. Enhanced low-level convergence supports a convective maximum over the plateau.

The SISO of convection over the plateau mainly consists of convection with strong diurnal variation. The area of active convection occurs within an anticyclonic circulation with relatively weak synoptic-scale winds. Further studies will be needed to solve the relationship between synoptic conditions and the local circulation over the plateau. The origin of the large-scale atmospheric circulation with a period of ~14 days, which modulates convective variability at the same timescale over the plateau, should also be investigated.

Acknowledgments

We thank Dr. H. Ueda of the University of Tsukuba for his thoughtful discussions and comments. Valuable comments and suggestions provided by Prof. F. Kimura and Prof. H.L. Tanaka of the University of Tsukuba and Prof. A. Kitoh of the Meteorological Research Institute (MRI) are gratefully acknowledged. Thanks are also due to Dr. N. Endo of the Frontier Research Center for Global Change (FRCGC) for helpful suggestions. The authors express their thanks to Dr. Y. Fukutomi of FRCGC and Mr. M. Hayasaki of the National Institute for Environmental Studies (NIES) for their helpful comments and providing some computational programs. GMS-IR data were provided by Dr. N. Yamazaki of MRI. The Generic Mapping Tools (GMT) graphics package developed by Wessel and Smith (1995) was used in preparing a part of the figures. This work was partially supported by a Grant-in-Aid for Scientific Research (A) (1), No. 14204044 from the Ministry of Education, Culture, Sports, Science and Technology, and by the Japan Science and Technology Agency (JST).

References

Ambrizzi, T., B.J. Hoskins and H.-H. Hsu, 1995: Rossby wave propagation and teleconnection patterns in the Austral winter. *J. Atmos. Sci.*, **52**, 3661–3672.

Annamalai, H. and J.M. Slingo, 2001: Active/break cycles: diagnosis of the intraseasonal variability of the Asian summer monsoon. *Clim. Dyn.*, **18**, 85–102.

Blackmon, M.L., Y.-H. Lee, J.M. Wallace and H.-H. Hsu, 1984: Time variation of 500 mb height fluctuations with long, intermediate and short time scales as deduced from lag-correlation statistics. *J. Atmos. Sci.*, **41**, 981–991.

Bolton, D., 1980: The computation of equivalent potential temperature. *Mon. Wea. Rev.*, **108**, 1046–1053.

Chen, T.-C. and J.-M. Chen, 1993: The 10–20-day mode of the 1979 Indian monsoon: Its relation with the time variation of monsoon rainfall. *Mon. Wea. Rev.*, **121**, 2465–2482.

Duchon, C.E., 1979: Lanczos filtering in one and two dimensions. *J. Appl. Meteor.*, **18**, 1016–1022.

Endo, N., K. Ueno and T. Yasunari, 1994: Seasonal change of the troposphere in the early summer of 1993 over central Tibet observed in the Tanggula mountains. *Bull. Glacier Res.*, **12**, 25–30.

Enomoto, T., B.J. Hoskins and Y. Matsuda, 2003: The formation mechanism of the Bonin high in August. *Quart. J. Roy. Meteor. Soc.*, **129**, 157–178.

Fujinami, H. and T. Yasunari, 2001: The seasonal and intraseasonal variability of diurnal cloud activity over the Tibetan Plateau. *J. Meteor. Soc. Japan*, **79**, 1207–1227.

——— and ———, 2002: Convective activity over the Tibetan Plateau and associated atmospheric circulation during GAME-Tibet IOP. *The second Tibetan Plateau experiment of atmospheric science*, China Meteorological Press, 118–121.

Fukutomi, Y. and T. Yasunari, 1999: 10–25 day intraseasonal variations of convection and circulation over East Asia and Western North Pacific during early summer. *J. Meteor. Soc. Japan*, **77**, 753–769.

——— and ———, 2002: Tropical-extratropical interaction associated with the 10–25-day oscillation over the western Pacific during northern summer. *J. Meteor. Soc. Japan*, **80**, 311–331.

Gilman, D.L., F.J. Fuglister and J.M. Mitchell, Jr., 1963: On the power spectrum of "Red Noise". *J. Atmos. Sci.*, **20**, 182–184.

Hartmann, D.L. and M.L. Michelsen, 1989: Intraseasonal periodicities in Indian rainfall. *J. Atmos. Sci.*, **46**, 2838–2862.

Hsu, H.-H. and S.-H. Lin, 1992: Global teleconnections in the 250-mb streamfunction field during the Northern Hemisphere winter. *Mon. Wea. Rev.*, **120**, 1169–1190.

Hsu, C.J. and R.A. Plumb, 2000: Nonaxisymmetric thermally driven circulations and upper-tropospheric monsoon dynamics. *J. Atmos. Sci.*, **57**, 1255–1276.

Kalnay, E. and Coauthors, 1996: The NCEP-NCAR 40-year reanalysis project. *Bull. Amer. Meteor. Soc.*, **77**, 437–471.

Kiladis, G.N. and K.M. Weickmann, 1992: Circulation anomalies associated with tropical convection during northern winter. *Mon. Wea. Rev.*, **120**, 1900–1923.

Krishnamurti, T.N. and P. Ardanuy, 1980: The 10 to 20-day westward propagating mode and "Breaks in the Monsoons". *Tellus*, **32**, 15–26.

——— and H.N. Bhalme, 1976: Oscillations of a monsoon system. Part I. observatinal aspects. *J. Atmos. Sci.*, **33**, 1937–1954.

——— and S. Gadgil, 1985: On the structure of the 30 to 50 day mode over the globe during FGGE. *Tellus*, **37**, 336–360.

Kurosaki, Y. and F. Kimura, 2002: Relationship between topography and daytime cloud activity around Tibetan Plateau. *J. Meteor. Soc. Japan*, **80**, 1339–1355.

Kuwagata, T., A. Numaguti and N. Endo, 2001: Diurnal variation of water vapor over the central Tibetan Plateau during summer. *J. Meteor. Soc. Japan*, **79**, 401–418.

Liebmann, B. and C.A. Smith, 1996: Description of a complete (interpolated) outgoing longwave radiation dataset. *Bull. Amer. Meteor. Soc.*, **77**, 1275–1277.

Madden, R.A. and P.R. Julian, 1972: Description of global-scale circulation cells in the Tropics with a 40–50 day period. *J. Atmos. Sci.*, **29**, 1109–1123.

Mitchell, J.M., Jr., 1966: Climate change. *Tech. Note 79*, World Meteorological Organization. 36–42.

Murakami, M., 1976: Analysis of summer monsoon fluctuations over India. *J. Meteor. Soc. Japan*, **54**, 15–31.

———, 1983: Analysis of the deep convective activity over the western Pacific and Southeast Asia. Part I: Diurnal variation. *J. Meteor. Soc. Japan*, **61**, 60–76.

———, 1984: Analysis of the deep convective activity over the western Pacific and Southeast Asia. Part II: Seasonal and intraseasonal variations during northern summer. *J. Meteor. Soc. Japan*, **62**, 88–108.

Murakami, T., 1981: Orographic influence of the Tibetan Plateau on the Asiatic winter monsoon circulation. Part IV. Long-period oscillations. *J. Meteor. Soc. Japan*, **59**, 201–219.

——— and J. Matsumoto, 1994: Summer monsoon over Asian continent and western North Pacific. *J. Meteor. Soc. Japan*, **72**, 719–745.

Nitta, T., 1983: Observational study of heat sources over the eastern Tibetan Plateau during the summer monsoon. *J. Meteor. Soc. Japan*, **61**, 590–605.

——— and S. Sekine, 1994: Diurnal variation of convective activity over the tropical western Pacific. *J. Meteor. Soc. Japan*, **72**, 627–641.

Popovic, J.M. and R.A. Plumb, 2001: Eddy shedding from the upper-tropospheric Asian monsoon anticyclone. *J. Atmos. Sci.*, **58**, 93–104.

Terao, T., 1998: Barotropic disturbances on intraseasonal time scales observed in the midlatitudes over the Eurasian Continent during the northern summer. *J. Meteor. Soc. Japan*, **76**, 419–436.

———, 1999: The zonal wavelength of the quasi-stationary Rossby waves trapped in the westerly jet. *J. Meteor. Soc. Japan*, **77**, 687–699.

Ueno, K., 1998: Characteristics of plateau-scale precipitation in Tibet estimated by satellite data during 1993 monsoon season. *J. Meteor. Soc. Japan*, **76**, 533–548.

Vincent, D.G., A. Fink, J.M. Schrage and P. Speth, 1998: High- and low-frequency intraseasonal variance of OLR on annual and ENSO timescales. *J. Climate*, **11**, 968–986.

Wessel, P. and W.H.F. Smith, 1995: New version of the Generic Mapping Tools released. *EOS, Trans. Amer. Geophys. Union*., **76**, 329.

Yanai, M. and C. Li, 1994: Mechanism of heating and the boundary layer over the Tibetan Plateau. *Mon. Wea. Rev.*, **122**, 305–323.

Yasunari, T., 1979: Cloudiness fluctuations associated with the Northern Hemisphere summer monsoon. *J. Meteor. Soc. Japan*, **57**, 227–242.

———, 1980: A quasi-stationary appearance of 30 to 40 day period in the cloudiness fluctuations during the summer monsoon over India. *J. Meteor. Soc. Japan*, **58**, 225–229.

———, 1981: Structure of an Indian summer monsoon system with around 40-day period. *J. Meteor. Soc. Japan*, **59**, 336–354.